Draft version March 5, 2018
Typeset using LaTeX **manuscript** style in AASTeX61

PROPER MOTION OF THE FAINT STAR NEAR KIC 8462852 (BOYAJIAN'S STAR) - NOT A BINARY SYSTEM

Dan P. Clemens,[1] Kush Maheshwari,[1,2,*] Roshan Jagani,[1,3,*] J. Montgomery,[1] A. M. El Batal,[1] T. G. Ellis,[4] and J. T. Wright[5]

[1] *Institute for Astrophysical Research, Boston University, 725 Commonwealth Ave, Boston, MA 02215*
[2] *Wayzata High School, Plymouth, MN*
[3] *North Hollywood High School, North Hollywood, CA*
[4] *Department of Physics & Astronomy, Louisiana State University, 261-A Nicholson Hall, Tower Dr. Baton Rouge, LA 70803-4001*
[5] *Department of Astronomy and Astrophysics, Pennsylvania State University, 424 Davey Lab, University Park, PA 16802*

ABSTRACT

A faint star located 2 arcsec from KIC 8462852 was discovered in Keck 10 m adaptive optics imaging in the JHK near-infrared (NIR) in 2014 by Boyajian et al. (2016). The closeness of the star to KIC 8462852 suggested the two could constitute a binary, which might have implications for the cause of the brightness dips seen by *Kepler* (Boyajian et al. 2016) and in ground-based optical studies (Boyajian et al. 2018). Here, NIR imaging in 2017 using the Mimir instrument resolved the pair and enabled measuring their separation. The faint star had moved 67 ± 7 milliarcsec (mas) relative to KIC 8462852 since 2014. The relative proper motion of the faint star is 23.9 ± 2.6 mas yr^{-1}, for a tangential velocity of 45 ± 5 km s^{-1} if it is at the same 390 pc distance as KIC 8462852. Circular velocity at the 750 AU current projected separation is 1.5 km s^{-1}, hence the star pair cannot be bound.

Keywords: stars: individual (KIC 8462852)

Corresponding author: Dan P. Clemens
clemens@bu.edu

[*] Boston University Research Internship in Science and Engineering (RISE) 2017 summer student

1. INTRODUCTION

The F3V star KIC 8462852 ("Boyajian's Star" (Deleted: ~~hereafter KIC 846~~)) at a distance of 390 pc (GAIA 2016) was found to be unusual by citizen-scientists examining *Kepler* light curves for the Planet Hunters program (Fischer et al. 2012). The star exhibited several strong brightness dips as well as families of lesser dips, with dip durations longer than typical of exoplanet transits (Boyajian et al. 2016, hereafter B16). Many models have been offered (see reviews by B16 and Wright & Sigurdsson (2016)), from alien megastructures (Wright et al. 2016), to swarms of nearly a thousand, co-traveling comets (Bodman & Quillen 2016), to dust-enshrouded massive objects on elliptical orbits (Neslušan & Budaj 2017), to twin collections of dusty systems of Trojan asteroids leading and following a planet with a tilted ring system (Ballesteros et al. 2018).

A fainter, possible companion, star (hereafter 'FS') was discovered in Keck Adaptive Optics (AO) observations conducted on 2014 October 16 in the near-infrared (NIR) J (1.25 μm), H (1.64 μm), and K-bands (2.20 μm) by B16. Optical speckle observations of KIC 8462852 did not detect FS, confirming its faint, red nature (B16). FS appeared 4.2 (J) to 3.6 (K) mag fainter than KIC 8462852, and was assigned a possible M2V classification by B16. They noted that the inferred large physical separation of FS from KIC 8462852 ($\sim$ 900 AU) meant the former star was unlikely to directly cause the deep brightness dips of the latter, though either a slow passage of FS through the system or a binary nature for the stellar pair could affect stability of bodies in the outer reaches of the KIC 8462852 system. The proximity of FS to KIC 8462852 arising from chance alignment of field stars was estimated by B16 to be $\sim$ 1%. The full nature of FS and its effects on the KIC 8462852 system remained unknown and in need of additional NIR observations, as optical imaging had proved unable to detect FS.

A 1.5-2% dip event for KIC 8462852, of six days duration, began on 2017 May 19 (Boyajian et al. 2017a), triggering optical monitoring of the stellar brightness at many observatories (Boyajian et al. 2018). Starting shortly thereafter, on May 25, the Mimir multi-function, NIR instrument (Clemens et al. 2007) was used to begin monitoring KIC 8462852 throughout the May/June/July period and on one night in November. These observations examined the KIC 8462852 system for NIR JHK

photometric variability, HK-band low-resolution spectroscopic properties, as well as H and K-band imaging polarimetry of KIC 8462852 and the other stars in its vicinity.

The NIR photometric variations, as well as the polarimetric and spectroscopic properties of KIC 8462852 resulting from these observations, are the subjects of related work (Clemens et al. 2018). This paper uses the Mimir data to develop astrometric findings regarding this stellar pair. Section 2 presents a summary of the Mimir observations and the data processing steps. Section 3 describes the analysis of the image data to isolate FS and measure its angular separation from KIC 8462852. Section 4 compares the measured relative proper motion for FS to the tangential velocity it would have in circular orbit about KIC 8462852 and assesses the impact of the findings. Section 5 recaps the study findings.

2. OBSERVATIONS AND DATA PROCESSING

NIR JHK observations were obtained using Mimir on the 1.8 m Perkins telescope, located outside Flagstaff, AZ on multiple nights spanning UT 2017 May 25 though July 06. A second set of observations was obtained on 2017 November 16. Mimir employed a 1024×1024 ALADDIN III InSb array detector, cooled to 33.5 K, with reimaging optics cooled to 65-70 K. The plate scale was 0.58 arcsec per pixel, resulting in a 10×10 arcmin field of view (FOV). Photometric imaging used the Mauna Kea Observatory NIR filter set (Tokunaga & Vacca 2005). Polarimetry additionally utilized a rotatable, cooled, compound half-wave plate (HWP), for each of the H and K-bands, to introduce polarization modulation and a fixed, cooled wire grid for analysis. All observations were auto-guided, scripted and under computer control, including telescope motions as well as filter and HWP orientation changes.

Imaging photometry for the first observing run consisted of single 2.5 s exposures in each waveband, obtained toward six sky-dither positions, offset by 15-20 arcsec. During May 25 through June 19, one set of JHK observations was obtained per night. During later nights of that run, a mix of one, two, or three observation sets were obtained each night. Average (Replaced: FWHM replaced with: full-width at half-maximum) seeing values were 1.50, 1.47, and 1.33 arcsec in the J, H, and K bands, respectively. For the November run, photometric imaging consisted of six sky-dithered exposures

of 10, 5, and 10 sec respectively in the JHK bands. Fifteen observations were conducted in each waveband. Average seeing values were 1.51, 1.37, and 1.30 arcsec in JHK.

Imaging polarimetry in the H-band ('H-pol') was performed on four nights in the May - July period and was performed in the K-band on two nights in that period. These observations used 5 sec (two May nights) or 10 sec (two June nights) integration times for each of sixteen HWP orientation angles at each of six sky-dither positions to comprise one observation. Multiple observations were obtained for two of the June nights. In-dome flat-fields obtained for each HWP orientation were used to calibrate, along with the same darks and linearity data as for photometry. The average seeing values were 1.36 and 1.58 arcsec for H-pol and K-pol, respectively.

The processing steps for Mimir polarimetry data were described in Clemens et al. (2012a) with calibration described in Clemens et al. (2012b). To summarize, the raw science data were transformed into linearized data, dark and flat-field images were similarly linearized, and the darks and flat-fields were used to correct the transformed data into science-ready images. These were grouped as 96-image observations to obtain astrometric image solutions using the positions of 2MASS (Skrutskie et al. 2006) stars present in each image. Stars found in each image were matched across images to obtain relative image shifts and photometric differences.

Photometric processing skipped many of the polarization steps, as all images were obtained without any HWP or wire grid present in the optical beam. Each six-position sky-dither image in each waveband was analyzed to find detected stars and to measure their positions and fluxes. These were matched to resolve sky transmission variations and to flag and reject images with poor seeing or high winds, prior to stacking and summing the images making up each observation.

Astrometric fitting of the stars found in the final summed images to the positions of 2MASS stars resulted in typical positional difference standard deviations of about $60 - 80$ mas (Clemens et al. 2012a). The plate scale and field rotation angle values were established with uncertainties of one part in 2,000 or less, contributing negligibly to the measured uncertainties in the relative angular separations and position angles of the two stars described in the following.

3. DATA ANALYSIS AND FINDINGS

FS, discovered two arcsec east of KIC 8462852 in the Keck AO observations of B16, appears as a distortion on the eastern side of the Mimir stellar profile of KIC 8462852, as seen in the zoomed portion of one of the H-band stacked images in Figure 1. That figure shows the relative center locations of FS and KIC 8462852, with a 5 arcsec reference indicated at lower right. Mimir data analysis tools include a (Replaced: PSF replaced with: point spread function (PSF)) modeling component that builds the master list of stars in the field using the multiple, blended star PSF fitting approach of DAOPHOT (Stetson 1987). For sufficiently long exposures or averages of many such exposures, the star finding, PSF modeling and stellar removal, and additional star finding processes enabled detection of FS in the Mimir images.

The ninety-six images making up each H-pol and K-pol observation, when stacked and summed, were sufficiently deep to enable reliable separation of FS from KIC 8462852 for twelve of the fourteen H-pol observations and for both K-pol observations. The 37 observations in each waveband for the short exposure photometric observations from the 2017 May/June/July observations yielded 29 detections of FS. The longer exposure 2017 November photometric observations allowed separating FS from KIC 8462852 for 40 of the 45 observations.

Collectively, the observations yielded 83 sets of equatorial coordinates for FS and for KIC 8462852. These were differenced for every observation to find relative RA and decl offsets. The offsets were grouped by exposure time and waveband (H-pol and K-pol were the exceptions that were grouped together) to yield seven data subsets for each of the RA and decl offsets. The gaussian natures of the offset distributions were examined with a boot-strapped Kolmogorov-Smirnov approach. This returned the likelihood that a data subset was not greatly different from a gaussian characterized by the mean and dispersion of the data. Eleven of the fourteen data sets had likelihoods exceeding 90%, while the lowest likelihood was 40%. The lower likelihood data subsamples showed somewhat more positional deviation outliers than for a normal distribution and also tended to have the shorter exposure times. The longer exposure data had likelihoods greater than 60% and well-constrained positional scatter. Hence, positional uncertainties within each data subset were set equal to the standard deviation of the relative offsets for that data subset, separately for RA and decl. The

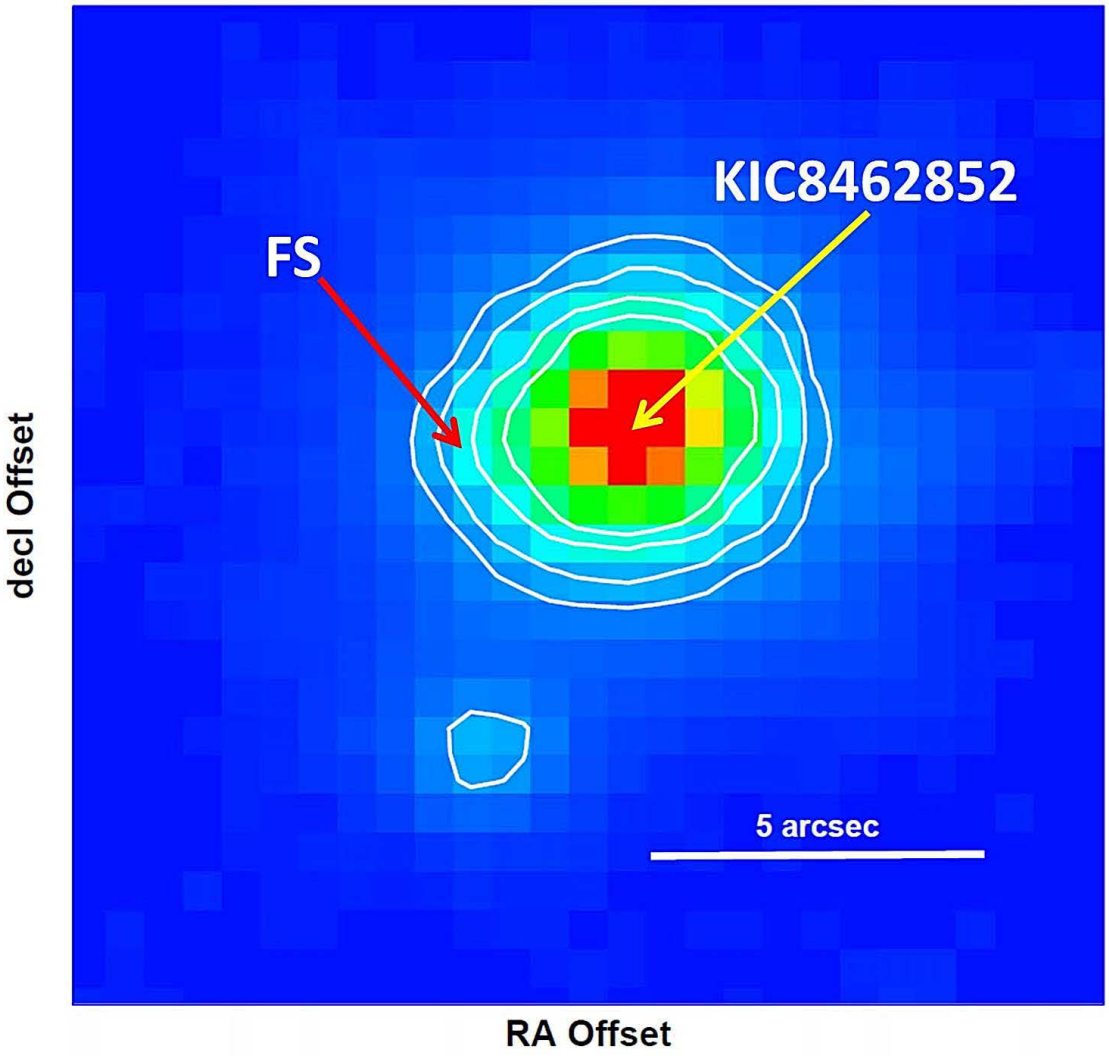

Figure 1. False color representation of a 15.5 × 15 arcsec portion of one of the Mimir H-band stacked observations, stretched to reveal the slight elongation to the east caused by the FS star on the side of the PSF of KIC 8462852. The two stars are separated by about 2 arcsec and a 5 arcsec reference angle is at lower right. Individual pixel sizes are 0.58 arcsec. White contours are stepped logarithmically to help show the eastward elongation.

inverse variances of these uncertainties were used as weighting factors when forming offset averages and propagated uncertainties. The offset standard deviations were smallest for the polarimetry data ($\sim 7-15$ mas; longest integration times), moderate for the longer exposure November photometry ($\sim 13-40$ mas), and largest for the short exposure photometry ($\sim 15-65$ mas).

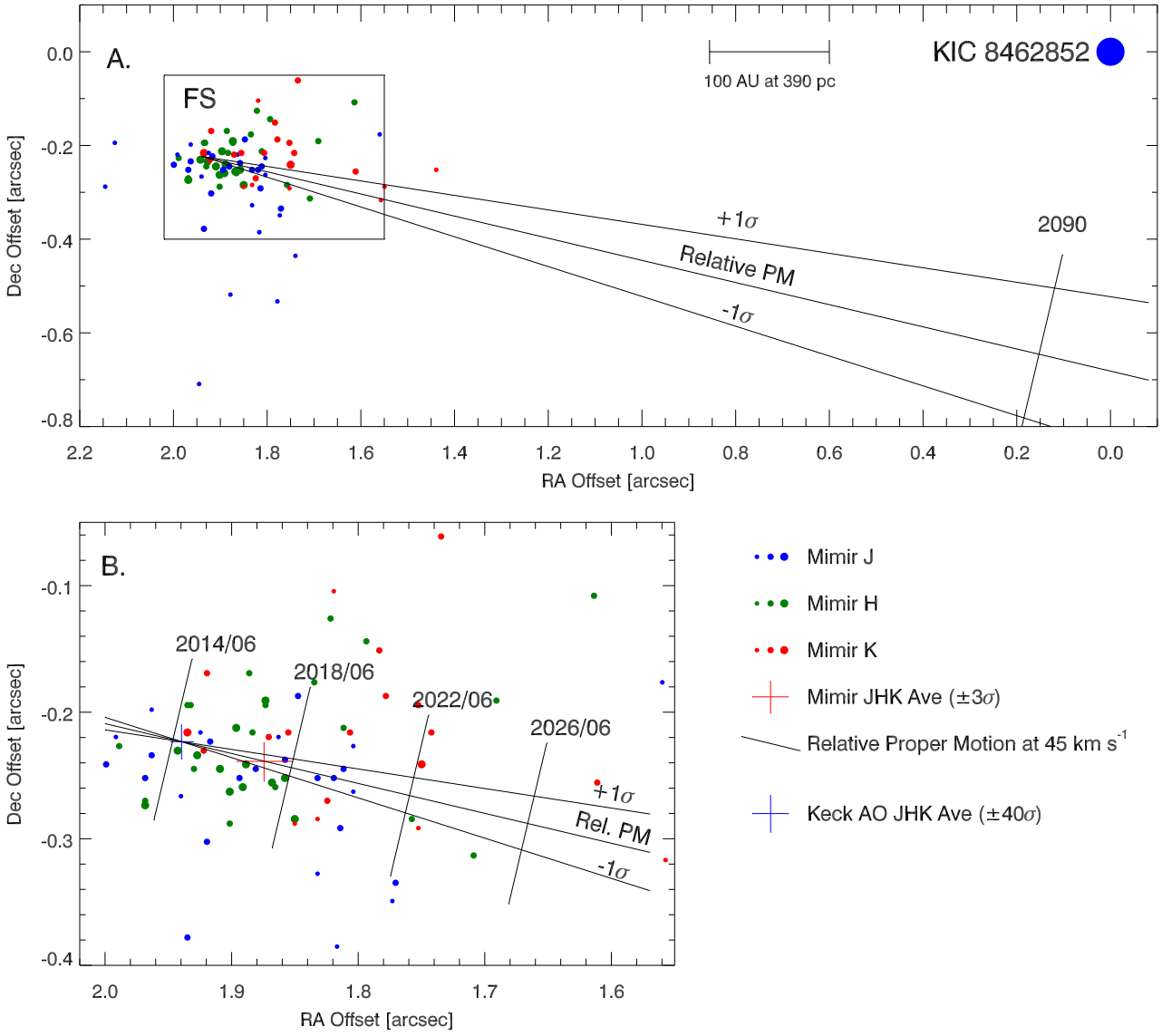

Figure 2. Sky offset positions for the faint star (FS) relative to KIC 8462852. Upper, A, panel shows that the relative offsets for FS, measured from Mimir data, are projected to lie some 750 AU southeast of KIC 8462852. A scale bar in the panel shows a length of 100 AU at 390 pc distance. The dashed line is the nominal relative proper motion vector. The dot-dashed lines show vectors offset by the uncertainty in the vector orientation. Along the nominal vector, closest approach to KIC 8462852 will happen in 2090, at a distance of about 260 AU. The lower, B, panel shows a zoomed view of the dotted rectangular region in Panel A. Filled small, colored circles in both panels represent measured Mimir relative offsets for FS. The average Mimir offset location and associated 3σ uncertainties are shown as the thick red cross. The average Keck AO JHK position (B16) and forty times its uncertainties (Boyajian 2017b) are shown as the thick blue cross. The dashed line shows the relative motion vector for 45 km s^{-1}, with perpendicular marks at four year intervals, on June centers. The proper motion measured corresponds to thirty times the circular velocity FS would have about KIC 8462852, if bound.

The relative positions measured for KIC 8462852 and FS are presented in Figure 2. The upper, A panel shows the Mimir-measured offsets, color-coded by waveband, with symbol size indicating the relative weighting (the largest symbols represent data with the most weight). The lower, B, panel shows a zoom of the dotted rectangular region in Panel A. In Panel B, the Keck AO position reported by B16, and updated with uncertainties from Boyajian (2017b), is shown as the thick blue error bars. These are 40 times the uncertainties of the Keck AO positions (Boyajian 2017b), to enable visualization. The weighted average offset and 3σ uncertainties for the Mimir observations are shown as the red cross. In addition to the nominal proper motion vector, vectors with position angles offset by 5° (1σ) are shown in both Figure panels. In the A panel, the date of closest projected approach for the nominal relative motion vector is 2090, at which time FS will be about 260 AU from KIC 8462852, if both are at 390 pc distance.

A mean position shift of FS relative to KIC 8462852 with observing waveband was found, and can be seen in the distributions of colored dots in Figure 2. The blue, J band dots have a tendency to be somewhat south and east of the H band dots while the red, K band dots continue that trend to be found mostly to the north and west. A variance-weighted fit returns a waveband-position vector with an equatorial position angle (EPA; measured east from north) of 307° of length 92 mas (K to J), with a SNR of about three. This is likely due to some combination of the interactions among the red color of FS, the detailed PSF structure in each waveband, and the sampled seeing and focus. As there is little astrophysical reason to believe a waveband-position gradient in the FS location should be present, and the gradient found is not highly significant, the FS location could either be reported as the fitted H band value, say, or the weighted average of the positions for all wavebands. These approaches return values identical to within a small fraction of their uncertainties, so the averaging method was adopted for simplicity.

The top portion of Table 1 presents the Mimir and Keck AO average relative offsets in both equatorial directions and as radial offsets and EPAs of FS from KIC 8462852. The bottom portion presents the differences in the KIC 8462852 to FS offset angles along the RA and decl directions between the Keck AO to Mimir observing dates. These yield an amplitude for the relative offset

Table 1. KIC 8462852 to Faint Star Projected Offsets

Property	Boyajian (2017b) Keck AO J H, K Ave.	This Work Mimir/Perkins J, H, K Ave.
Mean Julian Date Offset (relative to JD 2456947)	0	1,024
RA Offset [arcsec]	1.93957 (0.00023)	1.8743 (0.0073)
decl Offset [arcsec]	−0.22328 (0.00023)	−0.2388 (0.0051)
Radial Offset [arcsec]	1.95237 (0.00023)	1.8895 (0.0115)
Equatorial Position Angle [deg]	96.5667 (0.0067)	97.26 (0.16)
RA Offset Difference [mas]	65.3 (7.3)	
decl Offset Difference [mas]	15.5 (5.1)	
Offset Vector Amplitude [mas]	67.1 (7.2)	
Proper Motion Amplitude [mas yr^{-1}]	23.9 (2.6)	
Proper Motion EPA [° E of N]	256.7 (4.7)	
Tangential Speed (at 390 pc) [km s^{-1}]	44.9 (4.9)	

difference vector and the EPA of that vector. The effective date listed for the Mimir observations was formed from the average of the dates weighted separately for the RA and decl offsets, using the same weighting approach described above. Using this effective time separation between the Keck AO and Mimir observations, the relative proper motion amplitude was found to be about 24 mas yr^{-1}. Under the assumption that both stars are at the 390 pc distance, the tangential speed of FS, relative to KIC 8462852, was found to be 44.9 ± 4.9 km s^{-1}.

In Table 1 and in Figure 2, the Mimir RA uncertainties are larger than the decl uncertainties. This likely results from the uncertainty in the modeling and removal of the PSF of KIC 8462852, which overlaps FS significantly along the RA direction but less so along the decl direction.

4. DISCUSSION

The proper motion of KIC 8462852 has been reported by GAIA (2016), UCAC4 (Zacharias et al. 2012), and Tycho-2 (Høg et al. 2000). Weighted means of these reported values are -11.9 ± 0.5 mas yr^{-1} along RA and -10.2 ± 0.9 mas yr^{-1} along decl. These constitute a projected proper motion of 15.7 ± 0.7 mas yr^{-1} along EPA $229.^\circ4 \pm 2.^\circ5$ at a tangential velocity of 29.4 ± 1.3 km s^{-1}. These are similar to, but distinct from, the relative proper motion between FS and KIC 8462852 (45 km s^{-1} along EPA $\sim$260°). The projected vector sum results in absolute proper motions for FS of -35.3 ± 2.6 mas yr^{-1} along RA and -15.7 ± 2.0 mas yr^{-1} along decl, or 72 ± 5 km s^{-1} directed along EPA 246°.

The distance to FS may be resolved by GAIA observations, but that depends on its spectral type. If it is the M2V value suggested by B16, it should appear as a $V \sim 18$ mag object next to the 11.5 mag KIC 8462852. If, instead, the spectral type is M5.5V or later, its apparent optical magnitude may fall below the sensitivity limit of GAIA.

B16 also estimated the duration of passage of FS through the KIC 8462852 system, assuming identical distances and a relative motion of 10 km s^{-1}, to be of order 400 years. Here, the updated tangential speed is 4-5 times greater, yielding a much shorter passage. This should reduce the likelihood for scattering of objects from their outer KIC 8462852 system orbits that might have led to star-grazing or star-plunging comets or other bodies (Bailey et al. 1992; Lecavelier Des Etangs et al. 1999; Lecavelier Des Etangs 1999; Bodman & Quillen 2016).

The maximum circular orbit speed for FS, at the apparent projected 750 AU offset from KIC 8462852, would be 1.5 km s^{-1}. The Keck-to-Mimir tangential velocity for the pair at a common distance of 390 pc exceeds this value by a factor of thirty. The stellar pair cannot be bound and so do not constitute a binary.

5. SUMMARY

The relative proper motion of the faint star (FS) found within two arcsec of KIC 8462852 was measured relative to that brighter, and enigmatic, star by combining published Keck AO near-infrared imaging from 2014 with new Mimir near-infrared imaging from 2017. The relative separations of FS from KIC 8462852 were measured in 83 Mimir observation sets and combined to find that FS had moved by nearly 70 milli-arcsec over the three year interval. If FS is at the 390 pc distance to KIC 8462852, then the implied tangential velocity of 45 km s^{-1} and projected vector direction will put closest projected separation from KIC 8462852 at 260 AU about 70 years from now. The circular velocity at the projected 750 AU separation is only 1.5 km s^{-1}, which is much less than the implied tangential speed measured, if both stars are at the same distance. If the spectral type is significantly later than M2V, then FS is less distant and would be unrelated to KIC 8462852. In either scenario, the two stars are not in a bound pair, so models invoking KIC 8462852 brightness changes from interactions with FS are weakened.

The authors thank T. Boyajian and the anonymous reviewer for their comments and suggestions. The Boston University Research Internships in Science and Engineering (RISE) program for accomplished rising high school seniors selected and supported the participation of K.M. and R.J. on this project. This publication made use of data products from the Two Micron All Sky Survey, a joint project of the University of Massachusetts and the Infrared Processing and Analysis Center/California Institute of Technology, funded by NASA and NSF. This research was conducted in part using the Mimir instrument, jointly developed at Boston University and Lowell Observatory and supported by NASA, NSF, and the W.M. Keck Foundation. Support for the Mimir instrument and this scientific effort have been made possible by grants AST 06-07500, AST 09-07790, AST 14-12269 from NSF/MPS and NNX15AE51G from NASA to Boston University and by Perkins telescope observing time awarded as part of the Boston University – Lowell Observatory Discovery Channel Telescope partnership.

Facility: Perkins

REFERENCES

Bailey, M. E., Chambers, J. E., & Hahn, G. 1992, A&A, 257, 315

Ballesteros, F. J., Arnalte-Mur, P., Fernández-Soto, A., & Martínez, V. 2018, MNRAS, 473, L21

Bodman, E. H. L., & Quillen, A. 2016, ApJL, 819, L34

Boyajian, T. S., LaCourse, D. M., Rappaport, S. A., et al. 2016, MNRAS, 457, 3988 (B16)

Boyajian, T., Croft, S., Wright, J., et al. 2017, The Astronomer's Telegram, No. 10405

Boyajian, T. 2017, private communication (2017/10/06)

Boyajian, T., Alonso, R., Ammerman, A. et al. 2018, arXiv:1801.00732v1

Clemens, D. P., Sarcia, D., Grabau, A., et al. 2007, PASP, 119, 1385

Clemens, D. P., Pinnick, A. P., & Pavel, M. D. 2012b, ApJS, 200, 20

Clemens, D. P., Pinnick, A. P., Pavel, M. D., & Taylor, B. W. 2012a, ApJS, 200, 19

Clemens, D. P., Maheshwari, K., Jagani, R., et. al. 2018, in preparation

Fischer, D. A., Schwamb, M. E., Schawinski, K., et al. 2012, MNRAS, 419, 2900

GAIA Collaboration: Brown, A. G. A., Vallenari, A., Prusti, T.., et al. 2016, A&A, 595, A2

Høg, E., Fabricius, C., Makarov, V. V., et al. 2000, A&A, 355, L27

Lecavelier Des Etangs, A., Vidal-Madjar, A., & Ferlet, R. 1999, A&A, 343, 916

Lecavelier Des Etangs, A. 1999, A&AS, 140, 15

Mamajek, E. 2017, "A Modern Mean Dwarf Stellar Color and Effective Temperature Sequence", http://www.pas.rochester.edu/~emamajek/EEM_dwarf_UBVIJHK_colors_Teff.txt, Version 2017.10.19

Neslušan, L., & Budaj, J. 2017, A&A, 600, A86

Skrutskie, M.F., Cutri, R. M., Stiening, R., et al. 2006, AJ, 131, 1163.

Stetson, P. B. 1987, PASP, 99, 191

Tokunaga, A. T., & Vacca, W. D. 2005, PASP, 117, 421

Wright, J. T., Griffith, R. L., Sigurdsson, S., Povich, M. S., & Mullan, B. 2014, ApJ, 792, 27

Wright, J. T., Cartier, K. M. S., Zhao, M., Jontof-Hutter, D., & Ford, E. B. 2016, ApJ, 816, 17

Wright, J. T., & Sigurdsson, S. 2016, ApJL, 829, L3

Zacharias, N., Finch, C. T., Girard, T. M., et al. 2012, VizieR Online Data Catalog, 1322,